

Pattern formation via symmetry breaking in nonlinear weakly correlated systemsSuzanne M. Sears,^{1,2} Marin Soljačić,³ Demetrios N. Christodoulides,² and Mordechai Segev^{1,4}¹*Princeton University, Princeton, New Jersey 08544*²*Electrical Engineering and Computer Science Department, Lehigh University, Bethlehem, Pennsylvania 18015*³*Physics Department, Massachusetts Institute of Technology, Cambridge, Massachusetts 02139*⁴*Physics Department and Solid State Institute, Technion, Haifa 32000, Israel*

(Received 17 September 2001; published 7 March 2002)

We study pattern formation initiated by modulation instability in nonlinear partially coherent wave fronts and show that anisotropic noise and/or anisotropic correlation statistics can lead to ordered patterns.

DOI: 10.1103/PhysRevE.65.036620

PACS number(s): 42.65.Tg

The decay of signals and the growth of disorder are everyday occurrences in physical systems. Naively speaking, this is just a manifestation of the law of increase of entropy or second law of thermodynamics. Interestingly, however, in some circumstances order may appear spontaneously out of noise. Starting from an initially featureless background, random fluctuations may generate structures that naturally balance the various forces in the system and are stable. These may grow, as further fluctuations lead the system towards even more stable states. Such processes of ordered structures emerging from noise, or spontaneous pattern formation, are typically associated with phase-transition phenomena. In optics, spontaneous pattern formation has been demonstrated in many systems [1], in some cases arising from feedback, and in other occurring in the absence of feedback, i.e., during one-way propagation. Perhaps the best known example of pattern formation during unidirectional propagation is the process of modulation instability (MI), manifested as the breakup of a uniform “plane wave” [2] (or of a very long pulse in time [3]). Such an MI process can lead to the spontaneous creation of stable localized wave packets with particlelike features, namely, solitons, in nonlinear self-focusing media. Depending upon the nonlinear properties of the medium, perturbations of certain frequencies are naturally favored; these frequencies emerge out of white noise and gain in strength. These sinusoidal oscillations grow, becoming more and more peaky, until eventually the wave fragments into localized solitonlike wave packets. Until recently, MI was considered to be strictly a coherent process. But during the last two years, a series of theoretical and experimental studies [4–8] has demonstrated that modulation instability can also occur in random-phase (or weakly correlated) wave fronts, in both the spatial domain [4–8] and the temporal domain [9]. The main difference between MI in such partially coherent systems and the “traditional” MI experienced by coherent waves, is the existence of a threshold. In other words, in incoherent systems MI appears only if the “strength” of the nonlinearity exceeds a well-defined threshold that depends on the coherence properties (correlation distance) of the wave front. Thus far, incoherent MI has been demonstrated experimentally in both (1+1)D (one transverse dimension) [5,6,8] and (2+1)D (two transverse dimensions) [5,7] systems. Yet theoretically, analytic studies of incoherent MI were reported only for the (1+1)D case [4,8,9] and so far, the only theoretical work carried out in

(2+1)D systems has addressed a very different problem [7]. Furthermore, the experiments with (2+1)D incoherent MI [5,7,8] have left many open questions. For example, is there a threshold for (2+1)D incoherent MI? And if such a threshold exists, how does it relate to the threshold in (1+1)D systems? But beyond all other questions, the ability to explore (2+1)D incoherent MI adds another degree of freedom to the problem: anisotropy between the transverse dimensions that may lead to symmetry breaking and to the formation of asymmetric patterns. The anisotropy can arise from the nonlinearity, from the two-dimensional coherence function (that is, the correlation statistics of the random wave front), and interestingly enough, from the noise that serves as a “seed” for MI.

Here we formulate the theory of two-transverse-dimensional modulation instability in partially incoherent nonlinear systems, and study specific intriguing cases of broken symmetry between the two transverse dimensions. We show that quasicorrelated stripes, rolls, lattices, and gridlike patterns can form spontaneously from random noise in partially incoherent wave fronts in self-focusing noninstantaneous media. We show that the cases of broken symmetries (e.g., stripes and grids) can be generated by manipulating the correlation statistics of the incident wave front and/or by having anisotropic noise. We emphasize that, in fully coherent systems, the existence of features associated with broken symmetries is not surprising and has been demonstrated before [10]. But in partially incoherent (that is, random-phase and weakly correlated) systems, the very fact that anisotropy in the correlation statistics or in the statistics of the noise causes symmetry breaking and determines the evolving patterns is a new, exciting, and unique feature in the area of nonlinear dynamics and solitons.

We begin by considering a partially spatially incoherent optical beam propagating in the z direction that has a spatial correlation distance much smaller than its temporal coherence length; i.e., the beam is partially spatially incoherent and quasimonochromatic, and the wavelength of light λ is much smaller than either of these coherence lengths. The nonlinear material has a noninstantaneous response; the nonlinear index change is a function of the optical intensity, time averaged over the response time of the medium τ that is much longer than the coherence time t_c . Assuming the light is linearly polarized and that its field is given by $E(\mathbf{r}, z, t)$ [$\mathbf{r}=(x, y)$ being the transverse Cartesian coordinate vector],

we can define the associated mutual coherence function $B(\mathbf{r}_1, \mathbf{r}_2, z) = \langle E^*(\mathbf{r}_2, z, t)E(\mathbf{r}_1, z, t) \rangle$. The brackets denote the time average over time period τ . By setting

$$\mathbf{r} = \frac{(\mathbf{r}_1 + \mathbf{r}_2)}{2} = r_x \hat{x} + r_y \hat{y} = \frac{r_{1x} + r_{2x}}{2} \hat{x} + \frac{r_{1y} + r_{2y}}{2} \hat{y}$$

and

$$\boldsymbol{\rho} = (\mathbf{r}_1 - \mathbf{r}_2) = \rho_x \hat{x} + \rho_y \hat{y} = (r_{1x} - r_{2x}) \hat{x} + (r_{1y} - r_{2y}) \hat{y}$$

as the midpoint and difference coordinates $B(\mathbf{r}, \boldsymbol{\rho}, z)$ becomes the spatial correlation function in the new system. Note that $B(\mathbf{r}, \boldsymbol{\rho} = 0, z) = I(\mathbf{r}, z) = \langle |E(\mathbf{r}, z, t)|^2 \rangle$ where $I(\mathbf{r}, z)$ is the time-averaged intensity. We emphasize that in this model only time-independent perturbations can lead to MI; any rapid fluctuations will average out over the response time of the material τ and have no significant bearing on the final result. From the paraxial wave equation [4,11,12], we derive in (2+1)D an equation governing the evolution of the correlation function, $B(\mathbf{r}, \boldsymbol{\rho}, z)$,

$$\begin{aligned} \frac{\partial B}{\partial z} - \frac{i}{k} \left\{ \frac{\partial^2}{\partial r_x \partial \rho_x} + \frac{\partial^2}{\partial r_y \partial \rho_y} \right\} B \\ = \frac{in_0}{k} \left(\frac{\omega}{c} \right)^2 \left\{ \Delta n \left(r_x + \frac{\rho_x}{2}, r_y + \frac{\rho_y}{2}, z \right) \right. \\ \left. - \Delta n \left(r_x - \frac{\rho_x}{2}, r_y - \frac{\rho_y}{2}, z \right) \right\} B, \end{aligned} \quad (1)$$

where ω is the carrier frequency of the light, k is the carrier wave vector, n_0 is the index of refraction of the material without illumination, and Δn is the intensity-dependent nonlinear addition to the index of refraction ($|\Delta n| \ll n_0$).

MI is manifested in the development of a small intensity perturbation on top of an otherwise uniform beam. This can be expressed mathematically by taking $B(\mathbf{r}, \boldsymbol{\rho}, z) = B_0(\boldsymbol{\rho}) + B_1(\mathbf{r}, \boldsymbol{\rho}, z)$, where B_0 is the uniform beam B_1 is the perturbation to be affected by MI, and $|B_1| \ll B_0$. Substituting this latter form of B in Eq. (1) we obtain

$$\begin{aligned} \frac{\partial B_1}{\partial z} - \frac{i}{k} \left\{ \frac{\partial^2}{\partial r_x \partial \rho_x} + \frac{\partial^2}{\partial r_y \partial \rho_y} \right\} B_1 \\ = \frac{in_0}{k} \left(\frac{\omega}{c} \right)^2 \left\{ \kappa \left[B_1 \left[\left(r_x + \frac{\rho_x}{2}, r_y + \frac{\rho_y}{2} \right), (\rho_x = 0, \rho_y = 0), z \right] \right. \right. \\ \left. \left. - B_1 \left[\left(r_x - \frac{\rho_x}{2}, r_y - \frac{\rho_y}{2} \right), (\rho_x = 0, \rho_y = 0), z \right] \right] \right\} B_0(\boldsymbol{\rho}), \end{aligned} \quad (2)$$

where we have defined the marginal nonlinear index change evaluated at intensity I_0 , to be $\kappa = d[\Delta n(I)]/dI|_{I_0}$. Equation (2) is linear in B_1 and has translational invariance with respect to r . Thus B_1 can be investigated in terms of its plane-wave (Fourier) constituents, i.e., B_1 can be taken as proportional to $\exp[i(\alpha_x r_x + \alpha_y r_y)]$, where $\alpha_x = 2\pi/\Lambda_x$ and $\alpha_y = 2\pi/\Lambda_y$ are the wave vectors of the oscillations, and are

taken to be real. From the structure of Eq. (2), we expect that perturbations will grow exponentially with propagation distance z and so we assume B_1 to be proportional to $\exp(\Omega z)$, where Ω is the growth rate of the MI at a particular set of spatial wave vectors (α_x, α_y) . In fact, B_1 has to be exponential in z because of the translational invariance of Eq. (2) in z . Note that B_1 has no time dependence: any rapid perturbations will average out over the response time of the material τ . Thus, we can write the eigenmodes of Eq. (2) as

$$\begin{aligned} B_1 = \exp(\Omega z) \exp[i(\boldsymbol{\alpha} \cdot \mathbf{r} + \phi)] L(\boldsymbol{\rho}) + \exp(\Omega^* z) \\ \times \exp[-i(\boldsymbol{\alpha} \cdot \mathbf{r} + \phi)] L^*(-\boldsymbol{\rho}), \end{aligned} \quad (3)$$

where ϕ is an arbitrary real phase, and $L(\boldsymbol{\rho})$ are a set of modes that contain all the dependence on $\boldsymbol{\rho}$, and can be obtained for each (α_x, α_y) [4]. These eigenmodes satisfy $B_1(\mathbf{r}, \boldsymbol{\rho}, z) = B_1^*(\mathbf{r}, -\boldsymbol{\rho}, z)$, which is required from the definition of $B(\mathbf{r}, \boldsymbol{\rho}, z)$ given above. By introducing $M(\boldsymbol{\rho}) = L(\boldsymbol{\rho})/L(\boldsymbol{\rho} = (0,0))$ into Eq. (2) and integrating over z , we arrive at

$$\begin{aligned} \Omega M(\boldsymbol{\rho}) + \frac{1}{k} \left\{ \alpha_x \frac{\partial}{\partial \rho_x} + \alpha_y \frac{\partial}{\partial \rho_y} \right\} \\ \times M(\boldsymbol{\rho}) + \frac{2\omega\kappa}{c} \sin\left(\frac{\alpha_x \rho_x + \alpha_y \rho_y}{2}\right) B_0(\boldsymbol{\rho}) \\ = 0. \end{aligned} \quad (4)$$

Since growth can only occur for this form of the ansatz for B_1 if Ω has a real component greater than zero, we look for particular and homogeneous solutions to Eq. (4) for which this is the case. Physically, for growing modes, the homogeneous solution must be zero as $M(\boldsymbol{\rho})$ must be bounded for large $|\boldsymbol{\rho}|$. By taking the Fourier transform of Eq. (4) we find that

$$\begin{aligned} \hat{M}(k_x, k_y) = \left[\frac{i\omega\kappa/c}{\Omega - \frac{i}{k}(\alpha_x k_x + \alpha_y k_y)} \right] \left[\hat{B}_0 \left(k_x + \frac{\alpha_x}{2}, k_y + \frac{\alpha_y}{2} \right) \right. \\ \left. - \hat{B}_0 \left(k_x - \frac{\alpha_x}{2}, k_y - \frac{\alpha_y}{2} \right) \right]. \end{aligned} \quad (5)$$

where $\hat{F}(\mathbf{k}) = (1/2\pi)^2 \int_{-\infty}^{\infty} \int_{-\infty}^{\infty} d\boldsymbol{\rho} F(\boldsymbol{\rho}) e^{i\mathbf{k} \cdot \boldsymbol{\rho}}$ denotes the Fourier transform of $F(\boldsymbol{\rho})$. From the definition of $M(\boldsymbol{\rho})$ above, it can be seen that $M(\boldsymbol{\rho} = (0,0)) = L(\boldsymbol{\rho} = (0,0))/L(\boldsymbol{\rho} = (0,0)) = 1$. Using the inverse Fourier transform and this last condition one quickly finds that $\int_{-\infty}^{\infty} \int_{-\infty}^{\infty} dk_x dk_y \hat{M}(k_x, k_y) = 1$. Hence we arrive at the constraint,

$$1 = -\frac{\omega\kappa}{c} \int_{-\infty}^{\infty} dk_x \int_{-\infty}^{\infty} dk_y \times \left[\frac{\hat{B}_0\left(k_x + \frac{\alpha_x}{2}, k_y + \frac{\alpha_y}{2}\right) - \hat{B}_0\left(k_x - \frac{\alpha_x}{2}, k_y - \frac{\alpha_y}{2}\right)}{i\Omega + \frac{(\alpha_x k_x + \alpha_y k_y)}{k}} \right]. \quad (6)$$

Here, $\hat{B}_0(\mathbf{k})$ stands for the Fourier transform of $B_0(\boldsymbol{\rho})$ as expected, but note that this function also physically represents the angular power distribution of the beam. This can be seen by keeping in mind that $\boldsymbol{\theta}=(k_x/k, k_y/k)$ also represents the angle of propagation, as long as k_x and k_y are small compared to k . Once a form is chosen for $\hat{B}_0(\mathbf{k})$, Eq. (6) uniquely determines the growth rate Ω as a function of the wave vector (α_x, α_y) and contains all the information about how quickly the MI will grow and which spatial frequencies of perturbations will dominate.

We show now that if the radial symmetry in the transverse (x - y) plane is not broken, either by the medium or by the beam itself, many parallels can be drawn between the behaviors of the one- and two-transverse-dimensional systems. More specifically, the relation between the one- and two-dimensional growth rates, $\Omega_{2D}(\alpha_x, \alpha_y) = \Omega_{2D}(\sqrt{\alpha_x^2 + \alpha_y^2}) \equiv \Omega_{1D}(\alpha)$, can be shown to be true for any case in which the intensity of the beam is uniform and its correlation function is radially symmetric and separable: $\hat{B}_0(k_x, k_y) = \hat{B}_0(k_x)\hat{B}_0(k_y) = \hat{B}_0(|\mathbf{k}|)$. This separation is not just for mathematical convenience, but in fact separable correlation functions do exist in numerous physical settings. For example, transverse modulation instabilities of (1+1)D solitons in a 3D bulk medium can be eliminated by making use of a separable correlation function (although in that case the correlation function is also not radially symmetric) [11]. This implies that both the magnitude of the spatial frequencies of maximum growth and their corresponding growth rates must be identical in one- and two-transverse-dimensional systems. This important conclusion can be proven by the following argument. Since both the beam and the medium possess radial symmetry, the gain curve can have no dependence on angular orientation and thus must be a function only of the magnitude of $\boldsymbol{\alpha}$. Therefore, we may pick $\alpha_y=0$, $\alpha_x=\alpha$, and solve for the case $\alpha \geq 0$ without loss of generality. Rewriting the constraint Eq. (6) using this form for $\hat{B}_0(\mathbf{k})$ and these values for (α_x, α_y) , we see that

$$1 = -\frac{\omega\kappa}{c} \int_{-\infty}^{\infty} dk_y \hat{B}_0(k_y) \times \int_{-\infty}^{\infty} dk_x \left[\frac{\hat{B}_0\left(k_x + \frac{\alpha}{2}\right) - \hat{B}_0\left(k_x - \frac{\alpha}{2}\right)}{i\Omega + \frac{(\alpha k_x)}{k}} \right]. \quad (7)$$

Now since $\hat{B}_0(\mathbf{k})$ is identical with respect to k_x and k_y and normalized [i.e., $\int_{-\infty}^{\infty} \int_{-\infty}^{\infty} d\mathbf{k} \hat{B}_0(\mathbf{k}) = B_0(\boldsymbol{\rho}=(0,0)) = I_0$], integration over k_y further reduces this constraint to

$$1 = -\frac{\omega\kappa}{c} \int_{-\infty}^{\infty} dk_x \left[\frac{\hat{B}_0\left(k_x + \frac{\alpha}{2}\right) - \hat{B}_0\left(k_x - \frac{\alpha}{2}\right)}{i\Omega + \frac{(\alpha k_x)}{k}} \right] \quad (8)$$

where $\hat{B}_0(k)$ is now the one-dimensional normalized angular power spectrum. This is identical to that obtained in the (1+1)D case [4]. Therefore, since this equation gives the gain curve $\Omega(|\boldsymbol{\alpha}|)$, the curve itself, and all quantities derived from it, the wave vector of maximum growth α_{MAX} must be the same in both the (1+1)D and the (2+1)D cases.

To better understand the behavior of two-dimensional incoherent MI, we now consider a particular form of angular power spectrum, the double-Gaussian distribution,

$$\hat{B}_0(k_x, k_y) = \frac{I_0}{\pi k_{x0} k_{y0}} \exp\left[-\left(\frac{k_x^2}{k_{x0}^2} + \frac{k_y^2}{k_{y0}^2}\right)\right], \quad (9)$$

which is realizable experimentally. By numerically solving Eq. (6) for $\Omega(\alpha_x, \alpha_y)$, we find that the results are exactly identical to those obtained in the (1+1)D case using one-dimensional Gaussian statistics; i.e., the magnitude of the frequency of maximum growth and the growth rate as a function of frequency are the same in both one and two dimensions. These computations were performed using the coherent density approach [13,14] that describes the propagation of incoherent light in media with a noninstantaneous nonlinearity. In this model, infinitely many ‘‘coherent components’’ propagate at all possible angles [i.e., values of the wave vector (k_x, k_y)] and interact with one another through the nonlinearity that is a function of the time-averaged intensity. The shapes of the initial intensity profile for each of these coherent components are the same, but the relative weights are given by the angular power spectrum of the source beam, which is $\hat{B}_0(\mathbf{k})$, the Fourier transform of the correlation function. The nonlinear change in the refractive index is taken to be saturable and of the form $\Delta n = \Delta n_{\text{MAX}}[I_N/(1+I_N)]$, where Δn_{MAX} is the maximum nonlinear index change possible and $I_N = I/I_{\text{SAT}}$, I_{SAT} is the saturation intensity of the material.

Our numerical simulations (Fig. 1) confirm the analytic conclusion: the spatial frequency of maximum growth and its rate of growth are the same in (1+1)D and (2+1)D systems, provided that the nonlinearity, seed noise and the spatial correlation function are all fully isotropic. The (1+1)D case, [Fig. 1(a)] reveals strong peaks (the spatial frequency of maximum growth) occurring at $|\boldsymbol{\alpha}|/k = 0.035$, in accordance with the analytic theory. The (2+1)D case contains a ring of wave vectors [a side slice of which is shown in Fig. 1(b)] at $|\boldsymbol{\alpha}|/k = 0.0350$, exactly the same magnitude as in the (1+1)D case. The parameters chosen were $n_0 = 2.3$, $\lambda = 0.5 \mu\text{m}$, $k = 28.903 \mu\text{m}^{-1}$, $\Delta n_{\text{MAX}} = 5 \times 10^{-3}$, and $\theta_{0x} \equiv (k_{x0}/k) = \theta_{0y} = 13.85 \text{ mrad}$,

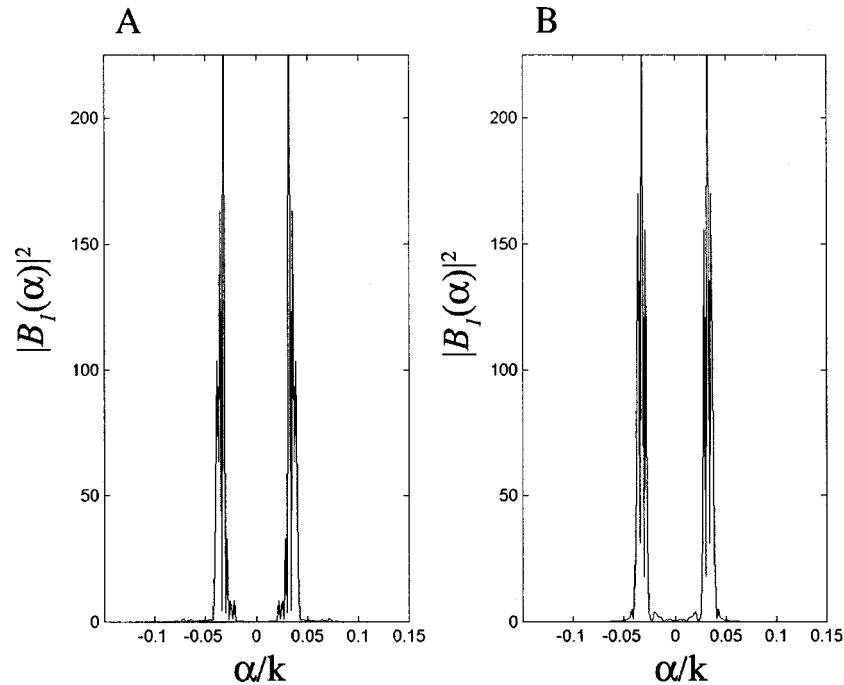


FIG. 1. (a) Comparison between the angular power spectra of the features resulting from incoherent modulation instability in the (1+1)D (a) and in the (2+1)D (b) cases, for a beam with the input power spectrum of Eq. (9) with $\theta_{0x} = 13.85$ mrad. The beam was propagated for 1.2 mm in a material with a saturable nonlinearity $\Delta n = \Delta n_{\text{MAX}}[I/(1+I)]$, where $\Delta n_{\text{MAX}} = 5.0 \times 10^{-3}$. The parameters used in both cases were identical, and only the number of spatial dimensions was varied. The figure shows the power spectrum (in arbitrary units) as a function of the transverse wave vector α normalized to the wave vector of the light k . The uniform incoherent background intensity has been subtracted out so that the statistics of the perturbations alone is shown. In (b), the results are radially symmetric, and we show a representative slice through the plane $\alpha_y = 0$.

which are representative of typical values in biased photorefractives. The input wave front was taken to be a very broad ($\sim 500 \mu\text{m}$), flat beam of height 1 in normalized units [with radial symmetry in the (2+1)D case], seeded with random Gaussian white noise [15] at a level of 10^{-5} . In both cases, the beams were allowed to propagate for 1.2 mm, and the intensity of the background beam was 1 in normalized units. As predicted by the theory, numerics confirm that the one- and two-dimensional cases grow at the same rates and at the same spatial frequencies. If the system is fully isotropic, that is, if the nonlinearity, input beam (both in its input intensity distribution and in its correlation function), and the noise, are all fully isotropic, then the (1+1)D case is fully equivalent to the (2+1)D case.

To conclude the section dealing with incoherent MI of input beams with isotropic properties (correlation function and seed noise), in fully isotropic nonlinear media, we emphasize that, because (2+1)D incoherent MI has no preference whatsoever with respect to any directionality in the transverse plane [as manifested by Eqs. (5)–(8)], the resultant patterns such as 1D stripes, 2D square lattices, and 2D triangular lattices, etc., all have the same growth rate and MI threshold. In other words, the system as it is does *not* differentiate between such patterns. This could lead to a naïve conclusion that all possible states of this system are equally likely to occur. But this conclusion is wrong: our simulations clearly indicate that, in spite of the fact that all possible 2D patterns in a fully isotropic system have the same threshold

for incoherent MI, some patterns are more likely to emerge than others. The reason for that is statistical: the likelihood for the emergence of filaments of a random distribution in space (for which the distribution in Fourier space is isotropic) is much greater than the likelihood of stripes (for which the peaks in Fourier space are lined up in some direction). Equally important, we note that our analytic calculation relies on a linearized stability analysis. After a long enough propagation distance, when the perturbations gain sufficiently high amplitudes, we expect that they will compete with one another, and some patterns will prevail over others, even if both have initially the same gain. In fact, our simulations reveal just that: some 2D structures emerge and others do not, even though they initially have the same gain.

Next we consider a case where the correlation function \hat{B}_0 is anisotropic, that is, the radial symmetry in the correlation statistics is broken: $\theta_{0x} \neq \theta_{0y}$ with the noise remaining fully isotropic. We will show that the extra spatial dimension allows for complex behaviors with no counterpart whatsoever in a one-dimensional system. In one dimension, it has been established that for sufficiently incoherent wave fronts, MI is totally suppressed [4]. In a 2D system with $\theta_{0x} \neq \theta_{0y}$, one may ask, what kind of features will emerge if the gain of the spatial frequencies in one direction is above the MI threshold, while the gain for those spatial frequencies in the other transverse direction are below threshold. To answer such questions, we must first derive constraints governing the on-

set of MI. Although the difference in behaviors above and below the threshold is very marked (MI either occurs or it does not) the transition between the two regimes is continuous, and so it must be that at this threshold both the gain Ω and its derivative $d\Omega/d|\alpha|$ are zero when $|\alpha|=0$ [4]. Let us first consider the threshold for MI to occur in the x direction, and set $\alpha_y=0$. For small values of α_x , Eq. (6) becomes (to first order in α_x)

$$1 = -\frac{\omega\kappa}{c} \int_{-\infty}^{\infty} dk_x \int_{-\infty}^{\infty} dk_y \times \left[\frac{\alpha_x \frac{\partial \hat{B}_0}{\partial k_x' k_x' = k_x}}{i \left(\Omega + \alpha_x \frac{\partial \Omega}{\partial \alpha_x' \alpha_x' = 0} + \frac{\alpha_x^2}{2} \frac{\partial^2 \Omega}{\partial \alpha_x'^2 \alpha_x' = 0} \right) + \frac{\alpha_x k_x}{k}} \right], \quad (10)$$

which reduces to

$$1 = -\frac{\omega\kappa}{c} \int_{-\infty}^{\infty} dk_x \int_{-\infty}^{\infty} dk_y \frac{1}{k} \frac{\partial \hat{B}_0}{\partial k_x' k_x' = k_x}. \quad (11)$$

Equation (11) can be solved exactly for k_{x0} , the threshold width of the angular power spectrum, for any form of the angular power spectrum $\hat{B}_0(\mathbf{k})$. Choosing the same double-Gaussian form as above [Eq. (9)], we find that MI will occur in the x direction if

$$\Delta n_{x\text{-threshold}} \equiv \kappa I_0 \geq \frac{n_0 k_{x0}^2}{2k^2}; \quad (12)$$

thus, if the nonlinearly induced index change Δn exceeds the threshold value on the right-hand side of Eq. (12), then MI will form stripes with periodicities (spatial frequencies) along the x direction. Since the initial constraint Eq. (6) is unchanged by interchanging k_x and k_y , it follows that y -direction MI must also be subject to a similar inequality,

$$\Delta n_{y\text{-threshold}} \equiv \kappa I_0 \geq \frac{n_0 k_{y0}^2}{2k^2}. \quad (13)$$

Although Eqs. (13) and (14) are identical functions with respect to k_{x0} and k_{y0} , there is no reason that the actual threshold values must be the same. It is, therefore, possible that if, for example, the beam is more coherent along the y direction than along the x direction, only MI with y directionality will occur. To test this analytic prediction, we use the coherent density approach [13,14] to simulate the propagation of a beam with ‘‘elliptical’’ double-Gaussian statistics, as in Eq. (9). The initial beam is more coherent in the y direction, with $\theta_{0y} = k_{y0}/k = 2.2$ mrad, but much more widely distributed in the x direction ($\theta_{0x} = k_{x0}/k = 9.6$ mrad). In the simulation, the input beam is a very wide ($\sim 500 \mu\text{m}$), flat, and radially symmetric wave front of intensity 1 in normalized units, with random Gaussian white noise added at a level of 10^{-5} . The

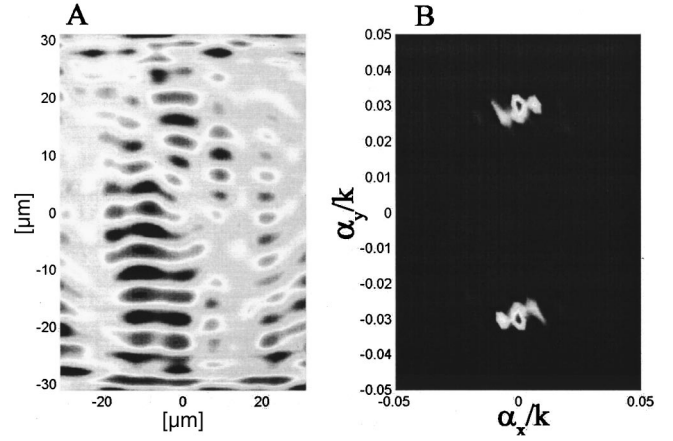


FIG. 2. Features resulting from incoherent modulation instability for an input beam of an elliptical double-Gaussian angular power spectrum [Eq. (9)] with $\theta_{0x}=9.6$ mrad and $\theta_{0y}=2.2$ mrad. The beam was propagated for 1 mm in material with a refractive index of the form $n=n_0+\Delta n_{\text{NL}} I$, where $n_0=2.3$ and $\Delta n_{\text{NL}}=5 \times 10^{-4}$. (a) shows the intensity of the perturbations, $|B_1(\mathbf{r})|^2$, in the spatial domain, with high intensity represented by white shading, low by dark. (b) shows the corresponding angular power spectrum $|B_1(\alpha)|^2$, where the uniform background intensity has been subtracted out.

beam is propagated for 1 mm in a material with a Kerr-type nonlinearity of the form $n=n_0+\Delta n_{\text{NL}} I_N$, where $n_0=2.3$ and $\Delta n_{\text{NL}}=5 \times 10^{-4}$. We find that the extra incoherence in the x direction inhibits the MI, as expected, and that the formation of stripes occurs preferentially in the more coherent y -direction. These results are presented in Fig. 2, where the emergence of MI in y and not in x is manifested in both the development of the spatial intensity fluctuations [Fig. 2(a) and in the corresponding Fourier spectra [Fig. 2(b)]. Figure 2(b) shows that a narrow band of wave vectors dominates the pattern formation process with significant MI occurring only for a very limited range of values for α_y/k (~ 0.03).

While the example of elliptical double-Gaussian correlation statistics begins to illustrate some of the variety that an extra spatial dimension can introduce, other forms for $\hat{B}_0(\mathbf{k})$ can lead to even more complex and completely different patterns. One interesting case that happens to be exactly solvable analytically is that of a partially incoherent optical beam with an angular power spectrum in the form of a double Lorentzian distribution

$$\hat{B}_0(k_x, k_y) = \frac{I_0 k_{x0} k_{y0}}{\pi^2 (k_x^2 + k_x^2) (k_y^2 + k_y^2)}, \quad (14)$$

which, while identical along the x and y directions, lacks radial symmetry and is narrower along the $\pm 45^\circ$ directions than along the 0° and 90° directions in the transverse plane. From this insight, one may naively expect that MI will appear first along the $\pm 45^\circ$ directions. But, in this case intuition is misleading. Using this particular form for $\hat{B}_0(\mathbf{k})$ in Eq. (6), one can then obtain exactly the gain curve $\Omega(\alpha_x, \alpha_y)$ that is,

$$\Omega(\alpha_x, \alpha_y) = - \left| k_{x0} \frac{\alpha_x}{k} \right| - \left| k_{y0} \frac{\alpha_y}{k} \right| + \sqrt{\alpha_x^2 + \alpha_y^2} \left(\frac{\kappa I_0}{n_0} - \frac{\alpha_x^2 + \alpha_y^2}{4k^2} \right)^{1/2}. \quad (15)$$

Equation (15) predicts that the strongest gain will occur along the 0° and 90° directions, and not along the 45° axis (as might be naively expected). Solving for the thresholds along the 0° ($\alpha_y=0$) and 45° directions and provided that ($\alpha_x = \alpha_y = k_0$), we find,

$$\Delta n_{45^\circ - \text{threshold}} \equiv \kappa I_0 \geq \frac{2n_0 k_0^2}{k^2} \quad \text{and}$$

$$\Delta n_{0^\circ, 90^\circ - \text{threshold}} \equiv \kappa I_0 \geq \frac{n_0 k_0^2}{k^2}. \quad (16)$$

Thus, the threshold value for the nonlinear index change $\Delta n_{\text{threshold}}$ is indeed lower along the 0° and 90° directions than along those tilted by 45° , even though the angular power spectrum is wider along the 0° and 90° directions than along the 45° tilted directions. In other words, in this intriguing example the *MI grows fastest along the directions with the widest angular distribution of power*, since it has the lowest threshold, and the winner takes it all. Such a phenomenon has no analog in (1+1)D, where *widening the angular power spectrum always decreases MI growth* [4]. Just why MI grows first along the directions with a wider distribution in k space (despite the intuition drawn from the 1D case) can be understood by considering the Fourier transform of the angular power spectrum, that is, the correlation function, $B_0(\mathbf{r}, \boldsymbol{\rho}, z)$. In general, in a 1D transform, a wider distribution in k space has a narrower distribution in r space, but in 2D this is not always the case and the actual geometry must be considered. In fact, the Fourier transform of a 2D double Lorentzian spectrum is broadest in r space (real space) along the same directions it is broadest in k space. So in fact, the beam is most strongly correlated along the 0° and 90° directions, even though these are the directions along which the angular power spectrum is the widest. From this example, it is apparent that MI grows preferentially in the most strongly correlated direction, and that this may or may not correspond to the direction with the most angularly concentrated distribution of the power.

We confirm these results using numerical simulations in the same material and beam parameters (n_0, λ, k) described above but with a saturable nonlinearity, $\Delta n = \Delta n_{\text{MAX}} [I/(1+I)]$, with $\Delta n_{\text{MAX}} = 1.8 \times 10^{-3}$. The input is a very broad ($800 \mu\text{m}$), flat wave front in the spatial domain, seeded with random Gaussian white noise at a level of 10^{-5} , with the degree of incoherence set by $\theta_{0x} = \theta_{0y} = 12 \text{ mrad}$. The results after 6 mm of propagation are shown in Figs. 3(a) and 3(b); the axis has been tilted by 20° to isolate any boundary artifacts of using a square grid to store data points. The result is just as predicted: MI occurs only on the 0° and 90° degree directions, as is evident in Fig. 3(b) that shows the power Fourier spectrum of the intensity perturbations, $|\hat{B}_1(\boldsymbol{\alpha})|^2$.

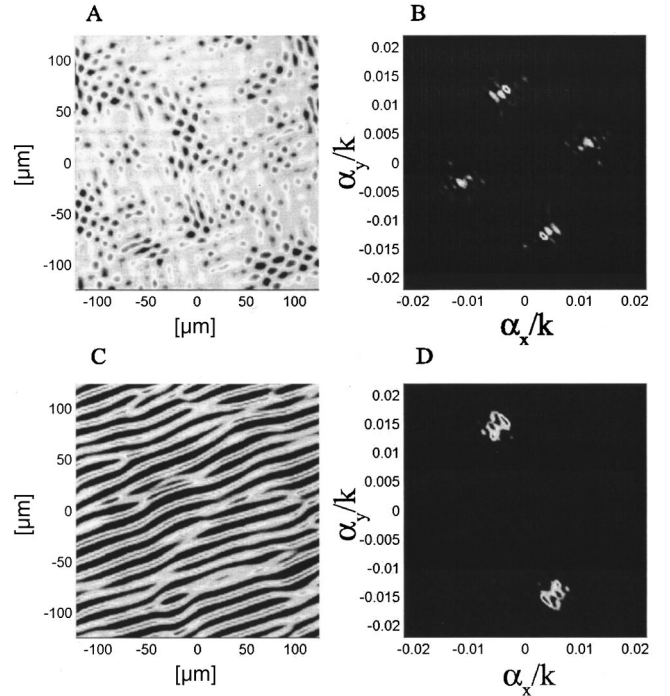


FIG. 3. Features resulting from incoherent modulation instability for an input beam of a double-Lorentzian angular power spectrum [Eq. (14)]. The beam was propagated for 6 mm in a material with a saturable nonlinearity of the form $\Delta n = \Delta n_{\text{MAX}} [I/(1+I)]$, with $\Delta n_{\text{MAX}} = 1.8 \times 10^{-3}$. (a) shows the intensity of the perturbations, $|B_1(\mathbf{r})|^2$ for $\theta_{0x} = \theta_{0y} = 12 \text{ mrad}$. The magnitude of the intensity is represented by the shading of the figure, with white representing maxima and black minima. (b) shows the corresponding angular power spectrum $|\hat{B}_1(\boldsymbol{\alpha})|^2$. (c) shows $|B_1(\mathbf{r})|^2$ for the $\theta_{0x} = 12 \text{ mrad}$ and $\theta_{0y} = 6 \text{ mrad}$. (d) shows $|\hat{B}_1(\boldsymbol{\alpha})|^2$.

The perturbations that experience highest gain occur near $|\boldsymbol{\alpha}|/k \sim 0.0125$, which compares well with 0.01, the value predicted by Eq. (15). We attribute this slightly lower value of the wave vector to neglecting higher-order terms in Eq. (2), where the intensity-dependent change in Δn , was approximated as $\kappa I_0 = d[\Delta n(I)]/dI|_{I_0} \times I_0$. This result is exact in the Kerr case ($\Delta n = \Delta n_{\text{NL}} I$), but for saturable nonlinearities, which is what we use in our simulation (and which is also encountered in experiments, otherwise the patterns emerging from the MI are unstable), the approximation introduces a small error in finding the spatial frequency that grows fastest. Going back to the spatial domain, the emerging MI pattern is manifested as a grid of localized wave packets; overlapping the stripes in the x direction with those in the y direction results in increased intensity at the intersections of the grid.

To further explore the emergence of incoherent MI when the correlation statistics are anisotropic, we again use the form of the angular power spectrum used in Fig. 3, but distort it so that the correlation function of the beam is stretched in one direction with respect to the other. In this particular example, the angular widths are $\theta_{0x} = 12 \text{ mrad}$ and $\theta_{0y} = 6 \text{ mrad}$, while all other parameters are kept the same as in the previous example (of Fig. 3(a) and (b), where $\theta_{0x} = \theta_{0y}$

=12 mrad). In this case, Eq. (15) predicts the formation of strong peaks in the Fourier domain on the y axis at the 90° and 270° marks at $|\alpha|/k=0.016$. As Figs. 3(c) and 3(d) show, the numerical simulations confirm the analytic prediction: significant MI forms only in the y direction near $|\alpha|/k \sim 0.017$ (again, as above, the axes have been tilted by 20° to isolate artifacts of using a square grid to store data points). Note, that in the spatial domain the patterns appear similar to those produced using elliptical statistics, but the Fourier analysis, depicted in Fig. 3(d), reveals that the range of frequencies present is actually much narrower, with little spread in either the x or y directions, and thus stronger striping is seen overall. The strong intensity stripes seen here are very similar to patterns observed experimentally in photorefractive crystals [5,8].

Until this point, we have only used input beams that are inherently asymmetric in their correlation statistics (coherence properties) to produce symmetry breaking. But, it is legitimate to ask: Can a beam that is radially symmetric and of perfectly isotropic coherence properties give rise to anisotropic MI, that is, to spontaneous formation of patterns that lack radial symmetry? For example, can such a fully radially symmetric beam transform into stripes or another geometrically ordered grid-type state? The answer lies in the propagation dynamics. Obviously, asymmetry or anisotropy in the nonlinear medium can give rise to such phenomena, as is the case for the photorefractive nonlinearity and for nonlinearities in liquid crystals. But there exists another alternative that is actually much more interesting: asymmetry can exist in the noise that seeds the MI process. For example, inorganic photorefractive crystals have striations that appear in the form of planes of index inhomogeneities. As a result, random variations in the index of refraction (noise) are much greater along the direction normal to these planes. We investigate this phenomenon of pattern formation from incoherent MI in the presence of anisotropic noise by propagating a perfectly isotropic wave front with a radially symmetric angular power spectrum in a medium with broken symmetry. To model these kind of irregularities, we seed our initial input to the numerical simulations with predominantly one-dimensional noise that fluctuates strongly in the y direction, while remaining almost constant across the x direction [16]. The medium had a saturable nonlinearity of the form $\Delta n = \Delta n_{\text{MAX}}[I/(1+I)]$, where $\Delta n_{\text{MAX}} = 3.3 \times 10^{-3}$; other parameters were the same as in the simulation shown in Fig. 1. The angular power spectrum of the beam was a double Gaussian, as in Eq. (9), with $\theta_{0x} = \theta_{0y} = 2.2$ mrad. The results are shown in Figs. 4(a) and 4(b), after 2 mm of propagation and we see that indeed the random yet anisotropic noise breaks the symmetry and gives rise to stripes in the preferential direction. The angular power spectrum of the perturbation $|B_1(\alpha)|^2$ shown in Fig. 4(b), reveals that the mechanism behind the symmetry breaking process that leads to striping is different from both the methods to produce striping studied above. It is apparent that there is an overall background of fluctuations as in the radially symmetric case, but the MI is dominated by a very strong preferential growth of stripes at $x=0$, with spreading in the y direction.

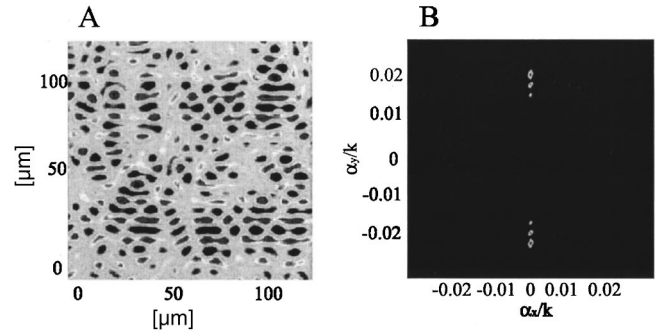


FIG. 4. Features resulting from incoherent modulation instability for an input beam with a radially symmetric Gaussian angular power spectrum (with $\theta_{0x} = \theta_{0y} = 2.2$ mrad), but with preferential (white) noise in the y direction that is 10^2 times stronger than the noise in the x direction. (a) shows the spatial distribution of the perturbation, $|B_1(\mathbf{r})|^2$, after 2 mm of propagation in a material with a saturable nonlinearity of the form $\Delta n = \Delta n_{\text{MAX}}[I/(1+I)]$, where $\Delta n_{\text{MAX}} = 3.3 \times 10^{-3}$, and (b) shows the corresponding angular power spectrum, $|B_1(\alpha)|^2$.

Before closing, we wish to note two generic results that links 2D to 1D systems. (I) Whenever the input beam has correlation statistics that are separable and radially symmetric as $\hat{B}_0(k_x, k_y) = \hat{B}_0(k_x)\hat{B}_0(k_y) = \hat{B}_0(|\mathbf{k}|)$, and the nonlinearity and the noise are fully isotropic, the features of 2D incoherent MI exactly reproduce those of 1D incoherent MI. The 2D system relates to the 1D system in a straightforward manner: the MI threshold and the growth rates are identical. (II) Whenever the input beam has correlation statistics that are separable but are *not* radially symmetric, such as $\hat{B}_0(k_x, k_y) = \hat{B}_{0x}(k_x)\hat{B}_{0y}(k_y) \neq \hat{B}_0(|\mathbf{k}|)$, and the nonlinearity and the noise are fully isotropic, the features of 2D incoherent MI can be mapped onto two independent 1D systems, corresponding to the two transverse dimensions, each of which having its own properties, such as MI threshold, growth rates, the spatial frequency off maximum growth, etc. We note, however, that these types of beams account for only a subset of all possible physical cases and the set of experiments that can be performed with two-dimensional partially incoherent beams. In fact, in many cases, either the correlation statistics are not separable, or anisotropic noise introduces directional preferences.

We have provided in this paper an analytical framework for studying $(2+1)$ D incoherent MI, and using numerical simulations, we have shown that the predictions of this theory are accurate. However, we may ask what will happen as the MI continues to grow. Are the patterns that evolve from incoherent MI stable or will they develop into something different? Or will they break apart? Initially the perturbations are only a very small sinusoidal wave on top of an otherwise uniform background. But perturbations that grow exponentially as the beam propagates must eventually reach the same order of magnitude as the background intensity $B_0(\rho)$ and the linearization assumption $|B_1| \ll |B_0|$ can no longer hold. Earlier works [5,7,8] have shown that as the MI grows large, the character of the dynamics changes, resulting in a transition from sinusoids on top of a constant background to individual, localized wave packets of increasing

height. The onset of this behavior can be seen in Fig. 4 above; the long thin ripples gradually become punctuated by small round peaks arranged in a gridlike structure; such grids have been observed experimentally [5,8]. The subsequent evolution of the system now depends on the nature of the nonlinearity and on the correlation statistics of the beam. In nonlinear Kerr media, the localized isolated peaks continue to grow in height and become narrower until a “collapse” occurs [17]. The system’s long-range evolution is completely different in saturable nonlinearities, where the isolated intensity peaks stabilize and remain mostly unchanged in shape by further propagation. The fact that incoherent MI in 2D saturable systems leads to a grid of isolated intensity peaks might be naively mistaken to be thought as a grid of localized islands of coherent, that is, possibly each isolated wave packet is an individual fully coherent (or fully correlated) entity. However, this is not the case: each of these isolated wave packets is still partially incoherent, albeit being slightly more coherent than the uniform beam that initiated them. Furthermore, the separation between two adjacent isolated wave packets is several times larger than the correlation distance. In the limit where this distance is not too large, long-range attraction forces between these localized wave packets lead to clustering of solitons, as was recently demonstrated experimentally and theoretically [7]. This means that the correlation statistics play a crucial role not only in determining the MI threshold and the dominating spatial frequencies, but also in determining the long-range evolution of the emerging patterns. This subject is described elsewhere [7], but for completeness, we briefly discuss the main ideas. When the initial beam is fully coherent and the nonlinearity is saturable, a stable grid of localized wave packets emerges. These wave packets propagate without further change in their width, i.e., they behave like quasisolitons. The interactions among these solitons are coherent, therefore, the interaction forces between adjacent localized wave packets can be either

attractive or repelling, depending upon the phase between them. Coherent MI, however, always produces features (quasisolitons) that are π out of phase with one another, thus, the dominating force between adjacent solitons is always repulsive. This leads to a grid of evenly spaced localized wave packets [5]. However, if the initial beam is sufficiently incoherent leading to incoherent MI, the phase-dependent interactions between and among the “MI products” (the localized isolated wave packets) that result from interference terms average out and only a net attractive force among these solitons survives. As a result, the solitons begin to draw nearer to their neighbors and cluster in aggregates of fine-scale structures: clusters of solitons [7].

In summary, we have studied theoretically modulation instability in $(2+1)$ D partially spatially incoherent systems. Our study reveals different and interesting dynamics that do not exist in $(1+1)$ D incoherent systems. In particular, we observe the ordering of the MI perturbations into stripes and grid-like features, which occurs if the symmetry of the system is broken in some manner. Some of these interesting dynamics of pattern formation from incoherent modulation instability have already been demonstrated experimentally in Refs. [5], [7], [8], but many other features are yet to be observed. Furthermore, such behavior should be observable in other natural systems, since solitons, MI, and incoherence are phenomena universal to many nonlinear systems. The discovery of incoherent MI has implications for many other nonlinear systems beyond optics. It implies that patterns can form spontaneously (from noise) in nonlinear many-body systems involving weakly correlated particles, such as, atomic gases at (or slightly above) the Bose-Einstein-Condensation temperatures.

This work was supported by the U.S. Army Research Office, and is part of the MURI program on optical spatial solitons. It was also supported by the NSF and the U.S. Air Force Office of Scientific Research.

-
- [1] F. T. Arecchi, S. Boccaletti, and P. Ramazza, *Phys. Rep.* **318**, 1 (1999).
- [2] E. M. Dianov *et al.*, *Opt. Lett.* **14**, 1008 (1989); P. V. Mamyshv *et al.*, *J. Opt. Soc. Am. B* **11**, 1254 (1994); M. D. Iturbecastillo *et al.*, *Opt. Lett.* **20**, 1853 (1995); M. I. Carvalho, S. R. Singh, and D. N. Christodoulides, *Opt. Commun.* **126**, 167 (1996).
- [3] V. I. Bespalov and V. I. Talanov, *JETP Lett.* **3**, 307 (1966); V. I. Karpman, *ibid.* **6**, 277 (1967); G. P. Agrawal, *Phys. Rev. Lett.* **59**, 880 (1987); S. Wabnitz, *Phys. Rev. A* **38**, 2018 (1988). A. Hasegawa and W. F. Brinkman, *IEEE J. Quantum Electron.* **16**, 694 (1980); K. Tai, A. Hasegawa, and A. Tomita, *Phys. Rev. Lett.* **56**, 135 (1981). For a review on modulation instability in the temporal domain, see G. P. Agrawal, *Nonlinear Fiber Optics*, 2nd ed. (Academic, San Diego, 1995), Chap. 5.
- [4] M. Soljacic, M. Segev, T. Coskun, D. N. Christodoulides, and A. Vishwanath, *Phys. Rev. Lett.* **84**, 467 (2000).
- [5] D. Kip, M. Soljacic, M. Segev, E. Eugenieva, and D. N. Christodoulides, *Science* **290**, 495 (2000).
- [6] J. Klinger, H. Martin, and Z. Chen, *Opt. Lett.* **26**, 271 (2000).
- [7] Z. Chen, S. M. Sears, H. Martin, D. N. Christodoulides, and M. Segev, *Proc. Natl. Acad. Sci.* (to be published).
- [8] D. Kip, M. Soljacic, M. Segev, S. M. Sears, and D. N. Christodoulides, *J. Opt. Soc. Am. B* **19**, 502 (2002).
- [9] B. Hall, M. Lisak, D. Anderson, R. Fedele, and V. E. Semenov, *Modulational Instability and Photon Landau Damping of Incoherent Light Wave Packets*, OSA Nonlinear Guided Waves Topical Meeting, Clearwater, FL, March 2001.
- [10] A. V. Mamaev, M. Saffman, A. A. Zazulya, *Phys. Rev. A* **54**, 870 (1996).
- [11] C. Anastassiou, M. Soljacic, M. Segev, E. Eugenieva, D. N. Christodoulides, D. Kip, Z. H. Musslimani, and J. P. Torres, *Phys. Rev. Lett.* **85**, 4888 (2000).
- [12] V. V. Shkunov and D. Z. Anderson, *Phys. Rev. Lett.* **81**, 2683 (1998).
- [13] D. N. Christodoulides, E. Eugenieva, T. Coskun, M. Segev, and M. Mitchell, *Phys. Rev. E* **63**, R35601 (2001).

- [14] D. N. Christodoulides, T. H. Coskun, M. Mitchell, and M. Segev, *Phys. Rev. Lett.* **78**, 646 (1997); **80**, 2310 (1998).
- [15] White noise was added in the frequency domain by adding a random number chosen from a Gaussian distribution separately to both the real and imaginary parts of each Fourier component. The width of the Gaussian distribution was chosen so that the average power added by the noise would be some small fraction of the total power, in our case 10^{-5} .
- [16] Unlike the previous simulations, here we also added noise in the spatial domain. A random number chosen from a Gaussian distribution was added separately to the real and imaginary parts of each component of the spatial profile. The noise was added first being held constant in the y direction; then another layer was added being held constant in the x direction. The ratio of the two layers of noise was 10^{-2} . An equal amount of noise was then added in the Fourier domain, consistent with the method used in Ref.[15]. The total power in the noise was 10^{-5} of the total.
- [17] N. N. Akhmediev, *Opt. Quantum Electron* **30**, 535 (1998).